Constraints on Skyrme equations of state from doubly magic nuclei, *ab initio* calculations of low-density neutron matter, and neutron stars

C. Y. Tsang,[1,*] B. A. Brown,[1,†] F. J. Fattoyev,[2,‡] W. G. Lynch,[1,§] and M. B. Tsang[1,‖]

[1]*Department of Physics and Astronomy and National Superconducting Cyclotron Laboratory, Michigan State University, East Lansing, Michigan 48824-1321, USA*
[2]*Department of Physics, Manhattan College, Riverdale, New York 10471, USA*

We use properties of doubly magic nuclei, *ab initio* calculations of low-density neutron matter and of neutron stars to constrain the parameters of the Skyrme energy-density functional. We find all of these properties can be reproduced within a constrained family of Skyrme parameters. The maximum mass of a neutron star is found to be sensitive to the neutron effective mass. A value of $[m_n^*/m](\rho_0) = 0.60$–0.65 is required to obtain a maximum neutron-star mass of 2.0 to 2.1 solar masses. Using the constrained Skyrme functional with the aforementioned effective mass, the predicted radius for a neutron star of 1.4 solar masses is 12.4(1) km and tidal polarizability is $\Lambda = 423(40)$.

Understanding the nature of dense neutron-rich matter is a major thrust of current research in both nuclear physics and astrophysics. Indeed a well-posed question of *"What is the nature of matter at extreme temperatures and densities?"* is regarded as a new scientific opportunity for the next decade [1]. To achieve this goal, many experiments and observations are being carried out using a wide variety of advanced new facilities, such as Facilities for Rare Isotope Beams, x-ray satellites, and gravitational wave detectors. In interpreting these experimental and observational results, the equation of state (EOS) of neutron-rich matter plays a critical role. Some parameters of the EOS that are crucial for neutron-star (NS) properties are not well constrained by nuclear reaction or structure experiments. In particular, the value of the neutron effective mass remains very uncertain [2,3]. In this Rapid Communication, we focus on the role of the neutron effective mass on the high-density EOS and show that it can be constrained using properties of doubly magic nuclei, *ab initio* calculations of low-density neutron matter in conjunction with astrophysical and gravitational wave observations. This, in turn, leads to constraining nuclear symmetry energy parameters and neutron skins of medium-to-heavy nuclei.

We start by mentioning the first direct detection of gravitational waves from the binary neutron-star merger GW170817 [4] that has already provided a fundamental new insight into the nature of dense matter. In particular, this detection provided critical properties of the neutron EOS that are encoded in the tidal deformability (also known as *tidal polarizability*)

of the neutron star, an intrinsic property of the star that describes its tendency to develop a mass quadrupole Q_{ij} in response to the tidal field induced by its companion E_{ij},

$$Q_{ij} = -\lambda E_{ij}, \tag{1}$$

where λ is the tidal deformability. By comparing point theoretical mass waveforms with the observed neutron-star merger waveform, the gravitational wave data analysis has also revealed the dimensionless tidal deformability Λ of a neutron star [4],

$$\Lambda \equiv \frac{\lambda c^{10}}{G^4 M^5} = \frac{2}{3} k_2 \left(\frac{c^2 R}{GM} \right)^5, \tag{2}$$

where k_2 is the second Love number [5,6]. The properties of neutron stars including the tidal deformability and the second Love number are sensitive to the EOS in the core and can be computed once the EOS is provided. For complete discussions on how to calculate tidal deformability please refer to Refs. [7–9]. In this Rapid Communication, we will use the constraint on the tidal deformability [10].

The structure of neutron stars is sensitive to the EOS of cold fully catalyzed neutron-rich matter over a range of densities spanning several orders of magnitude. For the low-density outer crust, we employ the EOS that follows the seminal work of Baym *et al.* [11]. In this region, the neutron-star matter consists of a Coulomb lattice of neutron-rich nuclei embedded in degenerate electron gas. As the density increases, the total chemical potential per nucleon of the system also increases and eventually exceeds the mass of a neutron.

At this point, the optimal nucleus cannot hold any more neutrons, and the neutron-drip point is reached which defines the interface between the outer crust and the inner crust [12]. The inner crust comprises the region from neutron-drip density $\rho = 4 \times 10^{11}$ g/cm^3, up to about half nuclear matter

*tsangc@nscl.msu.edu
†brown@nscl.msu.edu
‡ffattoyev01@manhattan.edu
§lynch@nscl.msu.edu
‖tsang@nscl.msu.edu

saturation density at which point the uniformity in the system is restored. On the top layers of the inner crust, the nucleons continue to be in the Coulomb crystal of neutron-rich nuclei embedded in the degenerate electron gas, which, however, is now also in chemical equilibrium with a superfluid neutron vapor. As the density increases further towards the core, the spherical nuclei that form the crystal lattice start to deform in an effort to minimize the Coulomb repulsion. As a result, the system is thought to exhibit rich and complex topological structures that emerge from a dynamical competition between the short-range nuclear attraction and the long-range Coulomb repulsion. The bottom layers of the inner crust, therefore, consist of complex and exotic structures, collectively referred to as *nuclear pasta* [13,14].

Due to the great number of quasidegenerate low-energy states, nuclear pasta systems display an interesting yet subtle low-energy dynamics that has been captured using either semiclassical simulations [15–23] or quantum-mechanical mean-field approaches [24–29]. In practice, one can resort to a cubic spline to interpolate between the outer crust and the uniform liquid interior which starts at densities of about half of the nuclear saturation. The neutron-star matter then undergoes a phase transition to a homogeneous liquid core where the Skyrme energy-density functionals (EDFs) are applied. More sophisticated crust calculations exist where interaction terms in the core region are used in the crustal calculation [30].

However, although some properties of neutron stars, such as "crustal radii" display strong sensitivity to the EOS of the inner crust [31], it has been shown that the *dimensionless* tidal deformability, in particular, is mostly sensitive to the EOS of the core almost independent of the detailed EOS of the inner crust [12]. Although it is important to have a consistent EOS of the crust and core, the exact form of the EOS of the crust does not affect the deformability [12,31,32]. Inclusion of a crust affects the NS radius as pointed out in Refs. [33,34], but the effect is small, a few hundred meters for the 1.4 solar mass neutron star with radii > 13 km and do not affect our conclusion or our results. Our approach should, therefore, yield a reliable result, even though we keep the complexity low.

For the neutron-star core, we use the EOS of cold neutron-rich matter derived from the nuclear Skyrme EDF describing the connection among the energy-density $\mathcal{E}$, the pressure P, and the baryon density ρ of the system. In addition, we assume that neutron-star matter is made of nucleonic matter complemented with electrons and muons in β equilibrium. The pressure of the system can either be found directly from the nuclear EDF plus leptonic contributions or from the energy density and its first derivative,

$$P(\rho) = \rho \frac{\partial \mathcal{E}(\rho)}{\partial \rho} - \mathcal{E}(\rho). \qquad (3)$$

Neutron stars satisfy the general relativistic stellar structure equations, also known as Tolman-Oppenheimer-Volkoff (TOV) equations,

$$\frac{dP(r)}{dr} = -G\frac{[\mathcal{E}(r) + P(r)][M(r) + 4\pi r^3 P(r)]}{r^2[1 - 2GM(r)/r]}, \quad (4a)$$

$$\frac{dM(r)}{dr} = 4\pi r^2 \mathcal{E}(r), \qquad (4b)$$

where G is the gravitational constant, r is the circumferential radius, and $M(r)$ is the gravitational mass content. Once an equation of state $[P = P(\mathcal{E})]$ is supplied, the TOV equations may be solved given boundary conditions in terms of a central pressure $P(0) = P_c$ and $M(0) = 0$. In particular, the mass M and the radius R are determined from the following two conditions: $P(R) = 0$ and $M = M(R)$. Once the TOV equations have been solved, the energy density and pressure profiles are obtained, one can then integrate the differential equation needed to obtain the tidal deformability [12]. This TOV solver has been used successfully to connect neutron-star properties to nuclear matter parameters in Skyrme interactions [33].

In this Rapid Communication, we focus on a particular family of the EOS model—the Skyrme EDFs—due to its versatility of being able to fit a myriad of nuclear observables [35]. In particular, it can be parametrized to not only reproduce properties of doubly magic nuclei, but also reproduce that of *ab initio* calculations, which are sensitive probes of the EOS in neutron-rich environments [2]. We start with the results obtained in Refs. [2,36]. In Ref. [35], an extensive study was performed to place constraints on EDFs based on the properties of nuclear matter. The standard form of the Skyrme EDFs and the parameters of the Skyrme functional are given in Ref. [35]. Out of 240 Skyrme EDFs, the 16 given in Table VI of Ref. [35] referred to as the CSkP set best reproduced a selected set of empirical nuclear matter properties. Five of these were eliminated since they gave transitions to spin-ordered matter around densities of $\rho = 0.25$ fm^{-3}. One of the remainder (LNS) produced unstable finite nuclei. The remaining ten are those listed in Table I and labeled with their names in Table VI of Ref. [35]. To this list, we added the commonly used SLy4 [37] and SkM* [38] functionals. These 12 EDFs provide a reasonable range of values for the symmetric nuclear matter (SNM) effective mass $[m_0^*/m](\rho_0) = 0.70$–$1.00(\rho_0 \approx 0.16$ nucleons/fm^3). The lower end of this range is that required by proton scattering on nuclei [39]. The upper end is the enhanced value required for the level density of single-particle energies near the Fermi surface due to the coupling with surface vibrations [39]. They also provide reasonable values for the nuclear incompressibility ($K_0 = 212$–242 MeV) as compared to values extracted from the energy of the giant monopole resonances ($K_0 = 217$–230 MeV) [40] and heavy-ion collisions at densities ranging up to $4.5\rho_0$ [41].

In Ref. [36], these 12 EDFs were refit to a common set of data for nuclear binding energies, charge radii, and single-particle energies from Ref. [42]. It was shown that the EOS for neutron matter and symmetry energy were constrained at 0.10 nucleons/fm^3 (about two-thirds of the nuclear saturation density for SNM). The slope of the neutron EOS at this density was not determined as was first pointed out in Refs. [43,44]. It was also first shown in Refs. [43,44] that the slope of the neutron EOS around a density of 0.10 nucleons/fm^3 was highly correlated with the neutron skin $R_{\text{skin}} = R_n - R_p$ of heavy nuclei, such as ^{208}Pb, where R_n and R_p are the root-mean-square radii for neutrons and protons, respectively.

TABLE I. Properties of the fitted Skyrme functionals. The symmetry energy J, its density derivative L, the symmetry-energy incompressibility K_{sym}, the symmetric-nuclear-matter incompressibility K_0, and effective-mass m_0^* are evaluated at $\rho_0 = 0.16$ fm^{-3}.

Name	σ	K_0 (MeV)	m_0^*/m	a_n (MeV fm^3)	b_n (MeV fm$^{3\gamma}$)	d_n (MeV fm^5)	J (MeV)	L (MeV)	K_{sym} (MeV)	R_{skin} (fm) ^{208}Pb	R_{skin} (fm) ^{48}Ca
KDE0v1	s3	1/6	217	0.81	−325	111	472	34.6	72	−40	0.200	0.178
NRAPR	s6	0.14	221	0.73	−316	84	489	34.1	70	−46	0.195	0.181
Ska25	s7	0.25	220	0.98	−281	37	465	31.9	59	−59	0.183	0.176
Ska35	s8	0.35	238	0.99	−274	32	467	32.0	58	−84	0.184	0.177
SKRA	s9	0.14	213	0.80	−347	143	426	33.4	65	−55	0.190	0.179
SkT1	s10	1/3	238	0.97	−283	50	476	32.6	63	−70	0.190	0.179
SkT2	s11	1/3	238	0.96	−279	46	470	32.6	62	−75	0.188	0.178
SkT3	s12	1/3	236	0.97	−275	32	467	31.9	58	−80	0.183	0.178
SQMC750	s15	1/6	223	0.75	−307	76	484	33.9	68	−50	0.194	0.180
SV-sym32	s16	0.30	232	0.91	−274	22	473	31.5	58	−77	0.181	0.179
SLy4	s17	1/6	222	0.76	−299	68	473	33.6	66	−55	0.191	0.179
SkM*	s18	1/6	219	0.79	−344	157	403	33.7	65	−65	0.187	0.179
Mean								33	65(7)	−63(24)	0.190(10)	0.178(3)

In Ref. [2], the same analysis was carried out with the additional constraint that the neutron EOS reproduced *ab initio* calculations of low-density neutron matter up to the E/N of 0.04 neutron/fm^3 [45–48]. The remarkable result of that paper was that the parameters of all 12 of the EDFs could easily be modified to be consistent with both the *ab initio* low-density neutron-matter calculations and the large set of nuclear data. The outcome was that the slope of the EOS could be tightly constrained; also, the neutron skins could be predicted. The largest remaining uncertainty was the neutron effective mass. In Ref. [2], a value of $[m_n^*/m](\rho_0) = 0.85$ was chosen, and the blue dashed curves in Fig. 1 represent the EOS of this family.

We start with this set of 12 Skyrme EDFs from Ref. [2] and calculate the properties of neutron stars. The mass-radius relationship and the deformability-radius relationship for 1.4 solar mass stars are shown as blue dashed curves in Figs. 2 and 3. The predicted values of the tidal deformability and radii for 1.4 solar mass stars shown as blue open symbols are within the constraints obtained from GW170817 [10] represented by a aqua shaded square in Fig. 3. However, the maximum mass obtained is 1.8(1) solar mass which is smaller than the 2.01(4) solar mass neutron star observed in Refs. [49,50] and the 2.14(10) solar mass neutron star observed in Ref. [51]. To reconcile the disagreement between our EDFs and this new condition, adjustment to EDFs' parameters is needed. By combining the gravitational and electromagnetic signals from GW170817, several interesting studies have been carried out to estimate the maximum mass of neutron stars that all suggest the absolute maximum mass of a neutron star to be about $\sim 2.24\,M_\odot$ [52–57].
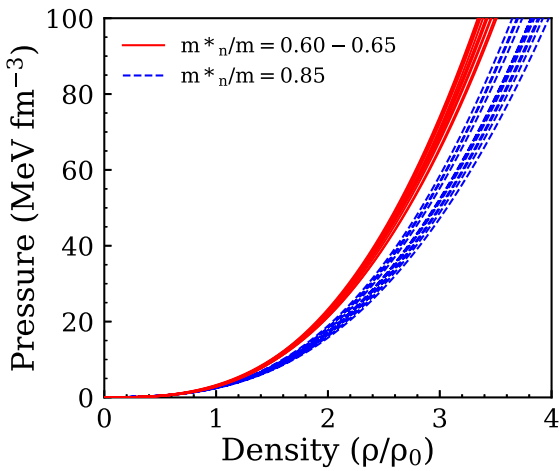

FIG. 1. The EOS in the form of pressure versus density used in this Rapid Communication. The red band corresponds to 12 Skyrmes with $m_n^*/m = 0.60$–65 (at ρ_0) whereas the blue band corresponds to 12 Skyrmes with $m_n^*/m = 0.85$. All EoSs are connected to a common crustal EoS [11] with crust-core transition density calculated using the empirical relation of Ref. [35].
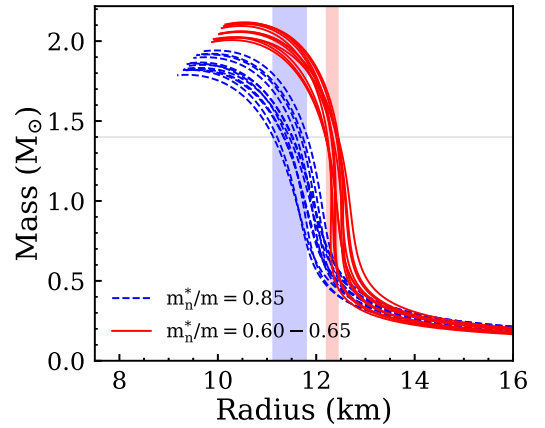

FIG. 2. Mass-versus-radius relation predicted by the two groups of Skyrme EoSs described in the text. The horizontal gray line indicates a value of 1.4 solar mass, and the two vertical bands show the range of intersections between the gray line and EoSs from each group, which corresponds to the range of predicted 1.4 solar mass neutron-star radius.
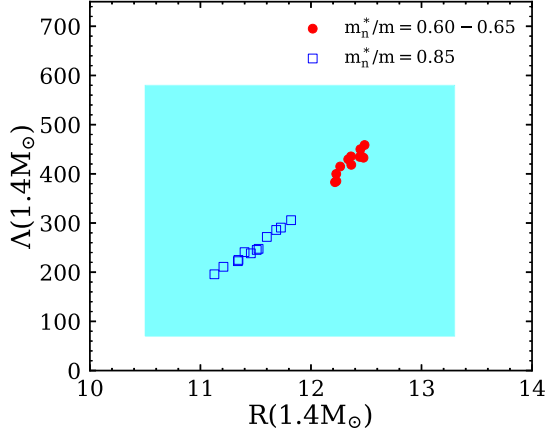
FIG. 3. Correlation between neutron-star tidal deformability and radii of the predicted 1.4 solar mass neutron star from two groups of Skyrmes (blue open square and red solid circle marker). The shaded aqua rectangular box in the background shows constraints from event GW170817 [10].

The Skyrme neutron EOS is given by the analytical expression [36],

$$\mathcal{E}(\rho) = a_n\rho^2 + b_n\rho^{2+\sigma} + c_n\rho^{5/3} + d_n\rho^{8/3}, \qquad (5)$$

where a_n, b_n, c_n, d_n, and σ are constants that depend on the Skyrme parameters. The first term is from the s-wave interaction, the second term is from the density-dependent s-wave interaction, the third term is the Fermi-gas kinetic energy, and the fourth term is from the p-wave interaction. The kinetic-energy contribution is the c_n term where $c_n = 119$ MeV fm^2.

The highest power of the density term d_n is related to the neutron-matter effective mass by

$$\frac{m_n^*(\rho)}{m} = \frac{c_n}{c_n + d_n\rho}. \qquad (6)$$

The next step was to refit the Skyrme parameters to all of the nuclear data and low-density neutron EOS constraints considered in Ref. [2] with the additional constraint that the maximum neutron-star mass comes out to be 2.0 to 2.1 solar masses. The outcome is that the neutron effective mass at ρ_0 is reduced from 0.85 to 0.60–0.65.

This change in the effective mass has little effect on quality of the fit to nuclear data or the low-density neutron EOS. For these 12 Skyrme functionals, the rms deviation for binding energies of ^{40}Ca, ^{48}Ca, ^{68}Ni, ^{88}Sr, ^{100}Sn, ^{132}Sn, and ^{208}Pb was 0.6–0.9 MeV, and the rms deviation for the root-mean-square charge radii of ^{40}Ca, ^{48}Ca, ^{88}Sr, and ^{208}Pb was 0.015–0.024 fm. Using the constrained Skyrme functional with the aforementioned effective mass, we obtain $L = 65(7)$ MeV for the density derivative of the symmetry energy at a density of $\rho_0 = 0.16$ nucleons/fm^3, neutron skins of $R_{\text{skin}}(^{208}\text{Pb}) = 0.190(10)$, and $R_{\text{skin}}(^{48}\text{Ca}) = 0.178(3)$ fm.

The results for neutron stars are shown as red solid curves in Figs. 1 and 2 and the red solid circles in Fig. 3. As shown in Fig. 1, the pressure difference between the results with

$[m_n^*/m](\rho_0) = 0.60$–0.65 and 0.85 for the neutron effective-mass groups are prominent at high density; $[m_n^*/m](3\rho_0) = 0.34$–0.38 and 0.65, respectively. It is possible that the effective-mass parameter in Skyrme is mocking up some aspect of dense neutron matter that cannot be extrapolated from normal nuclear density EOSs. In this case, the Skyrme phenomenology just provides a convenient and smooth functional form to be used for the neutron-star properties. It is important to note that all EOSs from both groups satisfy the causality condition. Their speed of sound never exceeds the speed of light for densities ranging up to the central density of its heaviest permitted neutron star.

When tidal deformability is inferred from our Skyrme EDFs, they show good agreement with gravitational wave observation as shown in Fig. 3. With the assumed Skyrme functional form and a neutron effective mass of 0.60–0.65 at ρ_0, the Λ and radius for 1.4 solar mass neutron stars can be narrowed down to 423^{+35}_{-40} and $12.4^{+0.1}_{-0.1}$ km, respectively.

In this Rapid Communication, we studied the effect of neutron effective mass, the largest source of EOS uncertainty from nuclear structure on neutron-star properties. $[m_n^*/m](\rho_0) = 0.60$–0.65 is required to produce a maximum mass of 2.0 to 2.1 solar masses. We showed that the tidal deformability Λ is sensitive to m_n^*/m, and due to this sensitivity, we were able to tighten the constraint on Λ using the Skyrme EDFs that satisfy our effective-mass condition. This effective-mass term, if correct, would strongly affect the neutron-star thermal properties, such as its heat capacity [58] as well as its neutrino luminosity [59–61]. Better knowledge of these thermal properties would contribute greatly to our understanding of the neutron-star cooling mechanisms [59]. More NS mergers are expected to be detected by the LIGO Collaboration, and it remains to be seen whether the new constraints converge to that from these Skyrme EDFs.

The connection of the maximum neutron-star mass, the neutron-star radius, and the neutron effective mass has also been recognized by Malik and co-workers [62,63]. In Ref. [63], they use the CSkP set of Skyrme interactions used in Ref. [36] without the further modifications made in Ref. [2], together with 13 more from Ref. [64]. They select those that best reproduce experimental data on the isoscalar and isovector modes of excitation in ^{208}Pb and the maximum mass for neutron stars. They, then, predict a radius $R(1.4\,M_\odot) = 11.6(10)$ km and a tidal deformability of $\Lambda(1.4\,M_\odot) = 267(144)$. The selected Skyrme interactions have effective masses with $[m_n^*/m](\rho_0) \approx 0.6$ and $[m_0^*/m](\rho_0) \approx 0.7$.

We start with the modified CSkP set obtained in Ref. [2] that gives a maximum neutron-star mass of 1.7–1.9 $M_\odot$. In Ref. [2], the neutron effective mass was rather arbitrarily constrained to have $[m_n^*/m](\rho_0) = 0.85$. Then, we constrain the neutron effective mass to have a smaller value of $[m_n^*/m](\rho_0) = 0.60$–0.65. This results in an increased maximum neutron-star mass of 2.0 to 2.1 $M_\odot$ which is in better agreement with observations. There is still a reasonably wide range of isoscalar effective masses (0.73–0.99) coming from the original CSkP parameter sets. With this change, we predict a radius of $R(1.4\,M_\odot) = 12.4(1)$ km and a tidal

deformability of $\Lambda(1.4\,M_\odot) = 423(40)$. These results are consistent with those of Malik *et al.*, but our uncertainties are smaller due to the constraint provided by the *ab initio* calculations of the low-density neutron-matter EOS from Ref. [2].

We note that the assumed functional form of the neutron EOS from the Skyrme EDFs provides the analytical connections between its properties inferred from nuclei (e.g., the value of the symmetry energy at a density of 0.10 nucleons/fm^3), those inferred from *ab initio* calculations of a low-density EOS of neutron matter, and those inferred for the high-density pressure of the neutron-matter EOS from the neutron-star radii. It will be important to see if any measured property of nuclei or neutron stars is inconsistent with our predictions. If so, then a less restrictive form [65] of the EOS will be required.

[1] D. Geesaman *et al.*, *Reaching for the Horizon; The 2015 Long Range Plan for Nuclear Science*, https://www.osti.gov/servlets/purl/1296778 (2015).

[2] B. A. Brown and A. Schwenk, Phys. Rev. C **89**, 011307(R) (2014); **91**, 049902(E) (2015).

[3] B.-A. Li, B.-J. Cai, L.-W. Chen, and J. Xu, Prog. Part. Nucl. Phys. **99**, 29 (2018).

[4] B. P. Abbott *et al.* (LIGO Scientific Collaboration and Virgo Collaboration), Phys. Rev. Lett. **119**, 161101 (2017).

[5] T. Binnington and E. Poisson, Phys. Rev. D **80**, 084018 (2009).

[6] T. Damour, A. Nagar, and L. Villain, Phys. Rev. D **85**, 123007 (2012).

[7] T. Hinderer, Astrophys. J. **677**, 1216 (2008).

[8] T. Hinderer, B. D. Lackey, R. N. Lang, and J. S. Read, Phys. Rev. D **81**, 123016 (2010).

[9] S. Postnikov, M. Prakash, and J. M. Lattimer, Phys. Rev. D **82**, 024016 (2010).

[10] B. P. Abbott *et al.* (LIGO Scientific Collaboration and Virgo Collaboration), Phys. Rev. Lett. **121**, 161101 (2018).

[11] G. Baym, C. Pethick, and P. Sutherland, Astrophys. J. **170**, 299 (1971).

[12] J. Piekarewicz and F. J. Fattoyev, Phys. Rev. C **99**, 045802 (2019).

[13] D. G. Ravenhall, C. J. Pethick, and J. R. Wilson, Phys. Rev. Lett. **50**, 2066 (1983).

[14] M. Hashimoto, H. Seki, and M. Yamada, Prog. Theor. Phys. **71**, 320 (1984).

[15] C. J. Horowitz, M. A. Perez-Garcia, and J. Piekarewicz, Phys. Rev. C **69**, 045804 (2004).

[16] C. J. Horowitz, M. A. Perez-Garcia, J. Carriere, D. K. Berry, and J. Piekarewicz, Phys. Rev. C **70**, 065806 (2004).

[17] C. J. Horowitz, M. A. Perez-Garcia, D. K. Berry, and J. Piekarewicz, Phys. Rev. C **72**, 035801 (2005).

[18] G. Watanabe, K. Sato, K. Yasuoka, and T. Ebisuzaki, Phys. Rev. C **68**, 035806 (2003).

[19] G. Watanabe, T. Maruyama, K. Sato, K. Yasuoka, and T. Ebisuzaki, Phys. Rev. Lett. **94**, 031101 (2005).

[20] G. Watanabe, H. Sonoda, T. Maruyama, K. Sato, K. Yasuoka, and T. Ebisuzaki, Phys. Rev. Lett. **103**, 121101 (2009).

[21] A. S. Schneider, C. J. Horowitz, J. Hughto, and D. K. Berry, Phys. Rev. C **88**, 065807 (2013).

[22] C. J. Horowitz, D. K. Berry, C. M. Briggs, M. E. Caplan, A. Cumming, and A. S. Schneider, Phys. Rev. Lett. **114**, 031102 (2015).

[23] M. E. Caplan, A. S. Schneider, C. J. Horowitz, and D. K. Berry, Phys. Rev. C **91**, 065802 (2015).

[24] A. Bulgac and P. Magierski, Nucl. Phys. **683**, 695 (2001).

[25] P. Magierski and P.-H. Heenen, Phys. Rev. C **65**, 045804 (2002).

[26] N. Chamel, Nucl. Phys. A **747**, 109 (2005).

[27] W. G. Newton and J. R. Stone, Phys. Rev. C **79**, 055801 (2009).

[28] B. Schuetrumpf and W. Nazarewicz, Phys. Rev. C **92**, 045806 (2015).

[29] F. J. Fattoyev, C. J. Horowitz, and B. Schuetrumpf, Phys. Rev. C **95**, 055804 (2017).

[30] P. H. F. Douchin, Astron. Astrophys. **380**, 151 (2001).

[31] J. Piekarewicz, F. J. Fattoyev, and C. J. Horowitz, Phys. Rev. C **90**, 015803 (2014).

[32] R. Gamba, J. S. Read, and L. E. Wade, arXiv:1902.04616.

[33] C. Y. Tsang, M. B. Tsang, P. Danielewicz, F. J. Fattoyev, and W. G. Lynch, Phys. Lett. B **796**, 1 (2019).

[34] H. Sotani, K. Iida, and K. Oyamatsu, Mon. Not. R. Astron. Soc. **470**, 4397 (2017).

[35] M. Dutra, O. Lourenco, J. S. Sa Martins, A. Delfino, J. R. Stone, and P. D. Stevenson, Phys. Rev. C **85**, 035201 (2012).

[36] B. A. Brown, Phys. Rev. Lett. **111**, 232502 (2013).

[37] E. Chabanat, P. Bonche, P. Haensel, J. Meyer, and R. Schaeffer, Nucl. Phys. A **635**, 231 (1998); Erratum: **643**, 441 (1998).

[38] J. Bartel, P. Quentin, M. Brack, C. Guet, and H. B. Hakansson, Nucl. Phys. A **386**, 79 (1982).

[39] J. P. Blaizot and B. L. Fridman, Nucl. Phys. A **372**, 69 (1981).

[40] L.-G. Cao, H. Sagawa, and G. Colo, Phys. Rev. C **86**, 054313 (2012).

[41] P. Danielewicz, R. Lacey, and W. G. Lynch, Science **298**, 1592 (2002).

[42] B. A. Brown, Phys. Rev. C **58**, 220 (1998).

[43] B. A. Brown, Phys. Rev. Lett. **85**, 5296 (2000).

[44] S. Typel and B. A. Brown, Phys. Rev. C **64**, 027302 (2001).

[45] K. Hebeler and A. Schwenk, Phys. Rev. C **82**, 014314 (2010).

[46] I. Tews, T. Kruger, K. Hebeler, and A. Schwenk, Phys. Rev. Lett. **110**, 032504 (2013).

[47] T. Kruger, I. Tews, K. Hebeler, and A. Schwenk, Phys. Rev. C **88**, 025802 (2013).

[48] A. Gezerlis, I. Tews, E. Epelbaum, M. Freunek, S. Gandolfi, K. Hebeler, A. Nogga, and A. Schwenk, Phys. Rev. C **90**, 054323 (2014).

[49] P. B. Demorest, T. Pennucci, S. M. Ransom, M. S. E. Roberts, and J. W. T. Hessels, Nature (London) **467**, 1081 (2010).

[50] J. Antoniadis, P. C. Freire, N. Wex, T. M. Tauris, R. S. Lynch *et al.*, Science **340**, 1233232 (2013).

[51] H. T. Cromartie *et al.*, Nat. Astron. (2019), doi:10.1038/s41550-019-0880-2.

[52] M. Ruiz, S. L. Shapiro, and A. Tsokaros, Phys. Rev. D **97**, 021501(R) (2018).

[53] M. Shibata, S. Fujibayashi, K. Hotokezaka, K. Kiuchi, K. Kyutoku, Y. Sekiguchi, and M. Tanaka, Phys. Rev. D **96**, 123012 (2017).

[54] E.-P. Zhou, X. Zhou, and A. Li, Phys. Rev. D **97**, 083015 (2018).

[55] L. Rezzolla, E. R. Most, and L. R. Weih, Astrophys. J. Lett. **852**, L25 (2018).

[56] N.-B. Zhang and B.-A. Li, Eur. Phys. J. A **55**, 39 (2019).

[57] G. Baym, S. Furusawa, T. Hatsuda, T. Kojo, and H. Togashi, Astrophys. J. **885**, 42 (2019).

[58] A. Cumming, E. F. Brown, F. J. Fattoyev, C. J. Horowitz, D. Page, and S. Reddy, Phys. Rev. C **95**, 025806 (2017).

[59] E. F. Brown, A. Cumming, F. J. Fattoyev, C. J. Horowitz, D. Page, and S. Reddy, Phys. Rev. Lett. **120**, 182701 (2018).

[60] M. Baldo, G. F. Burgio, H.-J. Schulze, and G. Taranto, Phys. Rev. C **89**, 048801 (2014).

[61] S. Reddy, M. Prakash, J. M. Lattimer, and J. A. Pons, Phys. Rev. C **59**, 2888 (1999).

[62] T. Malik, N. Alam, M. Fortin, C. Providência, B. K. Agrawal, T. K. Jha, B. Kumar, and S. K. Patra, Phys. Rev. C **98**, 035804 (2018).

[63] T. Malik, B. K. Agrawal, J. N. De, S. K. Samaddar, C. Providência, C. Mondal, and T. K. Jha, Phys. Rev. C **99**, 052801(R) (2019).

[64] N. Alam, B. K. Agrawal, M. Fortin, H. Pais, C. Providência, A. R. Raduta, and A. Sulaksono, Phys. Rev. C **94**, 052801(R) (2016).

[65] A. Bulgac, M. M. Forbes, S. Jin, R. N. Perez, and N. Schunck, Phys. Rev. C **97**, 044313 (2018).